J Mater Sci: Mater Med (2015) 26:215
DOI 10.1007/s10856-015-5538-8

BIOCOMPATIBILITY STUDIES

Effect of silver nanoparticle geometry on methicillin susceptible and resistant *Staphylococcus aureus*, and osteoblast viability

Lisa Actis[1] · Anand Srinivasan[1] · Jose L. Lopez-Ribot[2] · Anand K. Ramasubramanian[1] · Joo L. Ong[1]

Received: 29 August 2014 / Accepted: 3 July 2015 / Published online: 21 July 2015

Abstract Orthopedic implant failure as a result of bacterial infection affects approximately 0.5–5 % of patients. These infections are often caused by *Staphylococcus aureus* which is capable of attaching and subsequently forming a biofilm on the implant surface, making it difficult to eradicate with systemic antibiotics. Further, with the emergence of antibiotic-resistant bacteria, alternative treatments are necessary. Silver nanoparticles have received much attention for their broad spectrum antibacterial activity which has been reported to be both size and shape dependent. The purpose of this study was therefore to evaluate the effect of three different geometries on their effect on microbial susceptibility as well as evaluate their effect on bone cell viability. Silver nanoparticles of spherical, triangular and cuboid shapes were synthesized by chemical reduction methods. The susceptibility of *S. aureus* and methicillin-resistant *S. aureus* was evaluated a 24 h period and determined using a colorimetric assay. Further, the viability of human fetal osteoblast (hFOB) cells in the presence of the silver nanoparticles was evaluated over a period of 7 days by AlmarBlue fluorescence assay. hFOB morphology was also evaluated by light microscopy imaging. Results indicated that silver nanoparticle geometry did not have an effect on microbiota susceptibility or hFOB viability. However, high concentrations of silver nanoparticles (0.5 nM) conferred significant susceptibility towards the bacteria and significantly reduced hFOB viability. It was also found that the hFOBs exhibited an increasingly reduced viability to lower silver nanoparticle concentrations with an increase in exposure time.

✉ Lisa Actis
lisa.actis@gmail.com; lisa.actis@utsa.edu

[1] Department of Biomedical Engineering, The University of Texas at San Antonio, San Antonio, TX 78249, USA

[2] Department of Biology, The University of Texas at San Antonio, San Antonio, TX 78249, USA

1 Introduction

The use of medical devices has become ubiquitous with the treatment of several conditions in the medical field. With increasingly successful applications of these devices, their use has grown greatly in recent decades. The use of medical devices around the world was estimated to be approaching 500 million devices per year in 2007, with the numbers having grown since then [1]. These devices include partially intracorporeal implants such as urinary catheters, endotracheal tubes, external sutures, percutaneous electrodes, and orthopedic external fixation systems, as well as totally intracorporeal implants such as internal sutures, drug delivery systems, artificial vessels and valves, cochlear implants, and orthopedic prostheses. While the percent of indwelling implants that fail due to bacterial infection are low, the impact of these failures on the population as well as the accompanying cost to the national health care systems are becoming increasingly significant. With the number of infections approaching 1 million/year, the associated medical costs are around $3 billion each year in the US [2].

The increase in the number of infections is of further concern due to the bacteria's ability to adhere and subsequently form a biofilm once colonized on the implant surface. These bacterial biofilms are comprised of a three-dimensional architecture of microbial cells encapsulated in an exopolymeric matrix [3, 4]. In addition to compromising the functionality of the implant and affecting its integration

with the surrounding tissue by the recruitment of inflammatory cells, the infection also has the ability to become systemic [5]. Moreover, as a result of the exopolymeric matrix, bacteria growing in biofilms are highly resistant to small molecules such as antibiotics thus rendering conventional therapies ineffective [6]. Oftentimes, removal of the implant is required in order to eradicate the infection. In the case of orthopedic implants, this involves a two-step process in which the patient must wait several weeks after the implant has been removed before a replacement can be inserted [7]. Not only is this revision very expensive to the patient, costing approximately $14,000, but they must also endure pain, discomfort and increased hospitalization time as a result of the infected implant [7]. Moreover, the insertion of the replacement implant has an associated increased likelihood of infection [4]. Bacteria such as *S. aureus* and *Staphylococcus epidermidis* (*S. epidermidis*) are often the cause of infections in orthopedic implants, and the emergence of highly virulent strains such as methicillin resistant *S. aureus* (MRSA) has made the treatment of these infections increasingly difficult [8]. MRSA has become the most commonly isolated nosocomial bacterial pathogen in most of the world, affecting approximately 94,000 patients in 2005 and leading to 19,000 deaths [9]. With MRSA's ability to form biofilms on implants which further enhances its resistance to antibiotics, it has become even more important to find alternative methods to prevent implant infection.

New approaches are being taken in order to reduce the risk of infection in indwelling medical devices. The common approach of improving aseptic techniques during surgery has little known improvement in reducing the incidence of implant infections [1]. Thus, increasingly more implants have surface treatments aimed at reducing infection by reducing bacterial attachment and thus preventing biofilm formation. Several of these treatments involve the release of antibiotics from the implant surface [10]. However, the increasing numbers of antibiotic-resistant bacteria will render these treatments ineffective. Alternatives to antibiotics have thus been widely investigated. One alternative treatment that has gained much attention recently is the use of silver nanoparticles (AgNPs). These AgNPs are well known for exhibiting antimicrobial properties against a broad-spectrum of bacteria including gram-negative and gram-positive bacteria [11]. While the exact mechanism of action of AgNPs in antibacterial activity is not fully understood, it is known that AgNPs can attach to the surface of the bacterial membrane and disturb its proper functions, such as permeability and respiration. Moreover, AgNPs can penetrate inside the bacteria and cause further damage by interfacing with sulfur- and phosphorous-containing compounds such as DNA. AgNPs can also release silver ions that further contribute to their bactericidal effects by disrupting ATP production and DNA replication [12]. For this reason, bacterial resistance to AgNPs has not yet been reported. While this property has repeatedly been shown to be size-dependent, it has been suggested that the geometry of the nanoparticles also has an effect on their antimicrobial activity [12–15]. Using *Escherichia coli* (*E. coli*), Pal et al. concluded that rod-shaped nanoparticles exhibited no antibacterial activity, whereas antibacterial activities were reported for sphere- and triangle-shaped nanoparticles [10]. Although other geometries including cube-shaped AgNPs have also been reported to demonstrate antibacterial activity, their effect on *S. aureus* and MRSA as well as on mammalian cells have not demonstrated [12]. As such, with the goal of promoting maximum osteoblast viability while reducing biofilm formation, this study was aimed at evaluating the effect of sphere-, triangle- and cube-shaped AgNPs on human fetal osteoblast (hFOB) cell viability and morphology as well as reducing the viability of attached *S. aureus* and MRSA bacteria.

2 Materials and methods

2.1 Bacteria culture

Stored at −80 °C in glycerol stock, *S. aureus* strain (UAMS1) and MRSA strain (TCH1516) were cultured on tryptic soy agar (TSA) plates and incubated at 37 °C for 24 h. Both cells strains are clinical isolates reported with the ability to form biofilms under optimal conditions, as mentioned in this article. A loopful of cells from fully grown TSA plates was then subcultured in 20 ml of tryptic soy broth (TSB) (Fisher Scientific, Asheville, NC) and grown in an orbital shaker at 37 °C for 12–18 h.

2.2 Mammalian cell culture

hFOB cells (9th passage, Life Technologies) were cultured in cell culture medium consisting of Dulbecco's modified Eagles medium (DMEM) supplemented with 10 % fetal bovine serum (GIBCO, Life Technologies, Carlsbad, CA) and 1 % penicillin–streptomycin–amphotericin (Life Technologies, Carlsbad, CA) using T-150 cell culture flasks (Corning, Tewksbury, MA). The cells were maintained at 37 °C in humidified atmosphere of 5 % carbon dioxide, changing cell culture medium every 3 days.

2.3 Synthesis of silver nanoparticles (AgNPs) of different geometries

All chemicals used to synthesize the AgNPs were obtained from Sigma-Aldrich, St. Lous, MO. Two different methods

were used to synthesize the AgNPs. The triangle-shaped silver nanoparticles (tAgNPs) were prepared according to the method described by Metraux and Mirkin [16]. Briefly, 25 ml of 0.1 mM $AgNO_3$, 1.5 ml of 30 mM trisodium citrate, 1.5 ml of 0.7 mM PVP ($M_w \sim 29{,}000$) and 60 µl of 30 wt% hydrogen peroxide were vigorously mixed together by a magnetic stir bar in the dark. 250 µl of 100 mM sodium borohydride was then rapidly injected and the reaction was allowed to proceed for 60 min or until the final colloid mixture turned blue in color. The sphere-shaped silver nanospheres (sAgNPs) were prepared in a similar method to tAgNPs, with the exception that hydrogen peroxide was not added to the reaction mixture, resulting in a golden yellow-colored colloid. Both the tAgNP and the sAgNP colloids were then purified by centrifugation at 6000 rpm for 20 min and re-suspended in distilled water. The pellet was further washed three times with deionized water in order to remove excess silver ions.

Cube-shaped silver nanoparticles (cAgNPs) were prepared according to the method described by Sun and Xia [17]. Briefly, 5 ml of anhydrous ethylene glycol was heated to 150 °C for 1 h. 3 ml of 0.375 mM PVP ($M_w \sim 55{,}000$) in ethylene glycol was then added immediately followed by the addition of 3 ml 0.25 M $AgNO_3$ in ethylene glycol. The reaction mixture was heated for 7 min and then quenched by placing the vial containing the reaction mixture in a water bath held at room temperature. Next, the reaction mixture was transferred to a centrifuge tube along with ethanol used to rinse the reaction vial. The colloid was centrifuged at $2000\times g$ for 30 min, followed by re-suspending the pellet in distilled water and re-centrifuging at $9000\times g$ for 10 min. The supernatant was then removed and distilled water was added to re-suspend the nanoparticles.

AgNP concentration was determined based on the Beer–Lambert law that relates absorbance of light by a material to the concentration of the attenuating species of the material. Briefly, nanoparticle size was approximated using dynamic light scattering (DLS) (Malvern Instruments, Herrenberg, Germany), and UV–visible absorption spectra of the nanoparticles were recorded with the DU 720 Beckman Coulter UV–visible spectrophotometer (UV–Vis Spec) (Beckman Coulter Inc., Pasadena, CA) in a 1-cm cuvette. Using these measurements, the AgNP concentration was determined with an equation based on Mie theory and described by Yguerabide and Yguerabide [18]. The nanoparticle stock solutions were then diluted to the desired concentration and sterile-filtered. The synthesized silver nanoparticles were further characterized by scanning electron microscopy (SEM), and zeta potential. SEM samples were prepared by placing a drop of homogeneous suspension on a copper grid with a lacey carbon film and allowing it to dry in air followed by imaging with the Hitachi S5500 SEM (Hitahi Ltd., Tokyo, Japan). Zeta potential measurements of the AgNPs suspended in water were recorded with a Malvern Zetasizer Nano Range (Malvern Instruments, Herrenberg, Germany).

2.4 Bacterial susceptibility to AgNP

To prepare the inocula for examining the susceptibility of *S. aureus* and MRSA to the different AgNPs, cells harvested from overnight TSA cultures were washed twice and re-suspended in sterile phosphate-buffered saline (PBS). The cell suspension was adjusted to a density of 1×10^7 cells/ml in brain–heart infusion (BHI) (Fisher Scientific, Asheville, NC) supplemented with human serum (HS) (Life Technologies, Carlsbad, CA) to a final concentration of 10 % HS in BHI (BHI–HS). Bacteria inocula were added to the wells of a 96-well tissue culture polystyrene plate and incubated for 2 h to allow the cells to settle. The supernatant was then carefully removed and AgNPs of different geometries in BHI–HS was added; the concentrations of all AgNPs geometries ranged between 0.0005 and 0.5 nM. The bacteria were allowed to grow aerobically at 37 °C for 24 h. Subsequently, culture medium was removed, and in order to assess the viability of adhering bacteria, bacteria capable of forming biofilm, a viability stain solution of 9 ml BHI and 1 ml PrestoBlue (Life Technologies, Carlsbad, CA) was added to the wells and incubated for 20 min in the dark at 37 °C. Absorption was measured at 570 nm using a Synergy 2 Microplate Reader (BioTek, Friedrichshall, Germany).

2.5 SEM

In order to confirm the formation of biofilm with this culture method, bacteria inocula were cultured on glass coverslips in the same manner described above. After a 24 h incubation period, cells were fixed for SEM analysis. Briefly, cells were fixed with 2.5 % w/v glutaraldehyde in 0.1 M sodium cacodylate buffer (pH 7.4) solution for 2 h at 37 °C followed by 2 h incubation in 1 % w/v osmium tetroxide solution in 0.1 M sodium cacodylate buffer (pH 7.4). Samples were then rinsed with water and dehydrated by soaking in a series of ethanol solutions (a step gradient of 30, 50, 70, 90 and 100 % in water for 10 min each). Samples were then lyophilized overnight and subsequently coated with a gold/palladium alloy of approximately 10 nm thickness. SEM was performed with a Zeiss EVO 40 electron microscope (Carl Zeiss, Thronwood, NY).

2.6 Human fetal osteoblasts (hFOB) viability in the presence of AgNPs

24 h prior to AgNP exposure, the hFOB cells were seeded into 96-well plates at a cell density of 50,000 cells/ml to

allow for cell attachment. The cells were then exposed to AgNP in cell culture medium at concentrations ranging between 0.0005 and 0.5 nM. After 1, 3, and 5 days, cells were washed with sterile 1× PBS followed by the addition of 10 % AlmarBlue (Fisher Scientific, Asheville, NC) in cell culture medium. After 4 h incubation at 37 °C, fluorescence was measured using the Synergy 2 Microplate Reader (ex: 540–570 nm, em: 580–610 nm). Cell morphology was observed by compound light microscopy using a Leica DMIL LED compound microscope with an attached MicroPublisher 5.0 RTV camera (Leica, Wetzlar, Germany).

2.7 Statistical analysis

Characterization measurements of AgNPs were analyzed for significance using one-way analysis of variance (ANOVA) with a Tukey post hoc test (n = 3). Numerical data for groups tested over 24 h were analyzed for significance using one-way (ANOVA) with a Tukey post hoc test (n = 3). Significance between groups tested with the same nanoparticle geometry was determined by an unpaired *t* test. Data for groups tested for 5 days were analyzed for significance using two-way ANOVA with a Bonferroni post-test (n = 3). All experiments were performed in triplicate. All values were reported as the mean ± standard error, all statistical evaluations were two-tailed, the alpha levels for all tests were 0.05, and the threshold for significance was set at $P < 0.05$.

3 Results

3.1 Characterization of AgNPs

Using UV–visible spectroscopy, Fig. 1a shows the absorption spectrum of the synthesized silver nanoparticles, with the surface plasmon absorption band having a maximum of ~400, ~540, and ~430 nm indicating the presence of sAgNPs, tAgNPs, and cAgNPs, respectively. The successful synthesis of the different shaped AgNPs was further confirmed by scanning electron spectroscopy (SEM) imaging (Fig. 1b–d). Size measurements of AgNPs taken by DLS (Table 1) indicated a range between 28 and 75 nm in diameter. The cAgNP were significantly different in size from the tAgNP and sAgNP and had the largest size measurements. Zeta potential measurements for all AgNPs geometries ranged between −15.9 and −28.9 mV indicating stable colloidal suspensions.

3.2 *S. aureus* and MRSA susceptibility to AgNPs

Attached *S. aureus* and MRSA showed similar susceptibility profiles to the AgNPs (Fig. 2). Likewise, AgNP geometry had no significant effect on bacterial susceptibility of attached cells. All geometries of AgNP showed 0 % bacterial viability at the highest tested concentration of 0.5 nM, whereas lower concentrations did not show reduced bacteria viability of attached cells. While the difference is not significant, there is a trend of the attached MRSA having greater susceptibility to the cAgNP over the tAgNP, especially at 0.05 and 0.005 nM AgNP. Furthermore, while not significant, the effect of AgNP on MRSA susceptibility was observed to be more profound when compared to that on *S. aureus*. In Fig. 3, the SEM micrographs demonstrated that, in the absence of silver treatment, MRSA and *S. aureus* formed biofilms as evidenced by the morphology and three-dimentional architecture. As highlighted in the figure, one can observe the formation of exopolymeric matrix material, which is the inherent property of a "true" biofilm.

3.3 hFOB viability in the presence of AgNPs

As shown in Fig. 4, viability of hFOB to AgNPs did not depend on the geometry of the nanoparticles. It was observed that 0.5 nM AgNPs killed all cells after 24 h, whereas the lower concentrations did not significantly

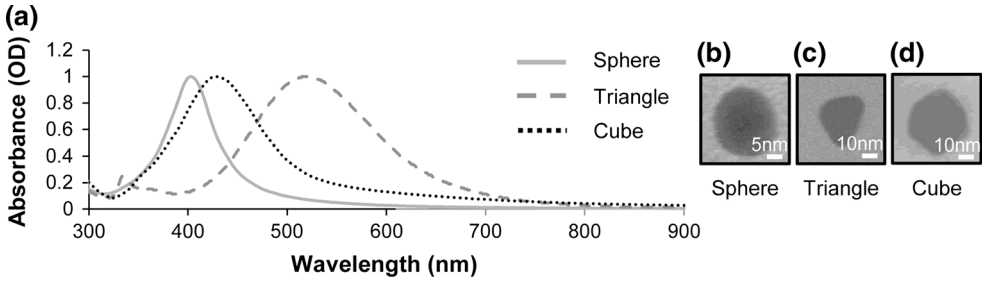

Fig. 1 Characterization of silver nanoparticles by UV/Vis and SEM; **a** UV/Vis spectrogram of sAgNP, tAgNP, and cAgNP with peaks at 400, 540, and 430 nm respectively; **b** representative SEM micrograph of sAgNP with a diameter of approximately 15 nm; **c** representative SEM micrograph of tAgNP with edge length of approximately 20 nm; **d** representative SEM micrograph of cAgNP with edge length of approximately 30 nm

reduce the number of live cells. However, after day 3, a concentration of 0.05 nM AgNPs was observed to reduce the hFOB population to approximately half that of the control group, and by day 5, all the cells had died. However, no reduction in the number of cells was observed as compared to the control group by day 5 in the presence of 0.005 and 0.0005 nM AgNPs concentration. Light microscope images (Fig. 5) show the change in cell morphology with the inclusion of high AgNP concentrations in cell culture media, whereas the low AgNP concentrations showed no effect on hFOB morphology, as indicated by the normal spreading patterns. Additionally, at higher AgNP concentrations, the cells were observed to have a more rounded morphology.

4 Discussion

In this work, AgNPs of different geometries, namely sphere-, triangle-, and cube-shaped nanoparticles, were synthesized. Their syntheses were immediately confirmed by the colorimetric change during the synthesis process. Colloids of sAgNP, tAgNP, and cAgNP result in a yellow-, blue- and green ochre-colored colloids respectively. The synthesis of the different geometries was further confirmed using UV–Vis spec and SEM. The spectra from UV–Vis spec is a function of the nanoparticle shape, size, media it is in, and the interparticle interactions [19]. The strong absorption band at around 400 nm by the sphere-shaped AgNPs had been reported to be characteristic for the spherical geometry, with the narrow band indicating nanoparticle size monodispersity [20]. The band also indicated that the particle had a size range of approximately 20–30 nm which was confirmed by DLS measurements [19]. The absorption band of 540 nm indicated the formation of triangle-shaped nanoparticles, with a broad band indicating variability in nanoparticle size [16, 21]. Finally, the absorption band at around 420 nm was observed for the cAgNPs, and such band had been reported to be characteristic for cubes of such small size [22]. Zeta potential measurements also revealed that the AgNPs were stable in water. The stability of the nanoparticles was reported to be attributed to the PVP coating which acted as a capping agent on nanoparticles [23]. It has also been reported that the addition of PVP mitigates aggregation in protein-containing cell growth media, a factor known to affect AgNP activity against bacteria [24].

Once the synthesis of the AgNPs was confirmed, their effects on the ability of *S. aureus* and MRSA to attach and thus form a viable biofilm were evaluated. It was observed that the susceptibility of MRSA to the AgNPs was higher than that of *S. aureus*. After a 24 h exposure, MRSA exhibited a 75 % reduction in adhered population as compared to the control at the lowest concentration of 0.0005 nM, whereas the adhered *S. aureus* population remained unchanged compared to control. As the concentration of AgNPs was increased, the susceptibility of *S. aureus* was observed to remain unchanged except at the highest concentration of 0.5 nM. This observation

Table 1 Zeta potential and hydrodynamic diameter measurements taken of sAgNP, tAgNP, and cAgNP

	Zeta potential (mV)	Hydrodynamic diameter (nm)
sAgNP	−15.91 ± 0.67*	34.10 ± 3.18[a]
tAgNP	−21.67 ± 1.10*	28.80 ± 4.89[a]
cAgNP	−28.90 ± 2.05*	75.29 ± 7.15

Significance of $*P < 0.001$

[a] Groups that are statistically the same

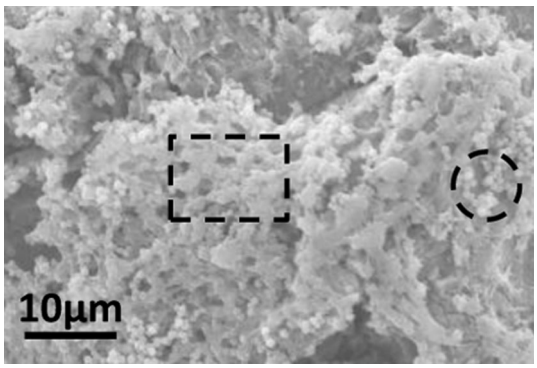

Fig. 3 SEM micrograph of MRSA biofilm formed after 24 h; the *circle* highlights the grape-like cluster of cells and the *rectangle* highlights the exopolymeric matrix characteristic of a biofilm

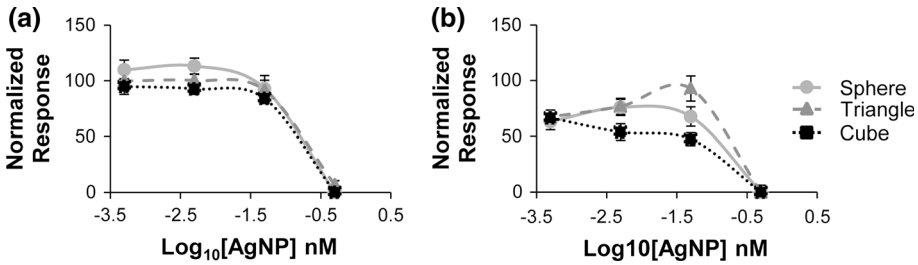

Fig. 2 Susceptibility, normalized to the control, of **a** *S. aureus* (UAMS1) and **b** MRSA (TCH1516), to sAgNP, tAgNP, and cAgNP over a range of concentrations between 0 and 0.5 nM after a 24 h exposure period

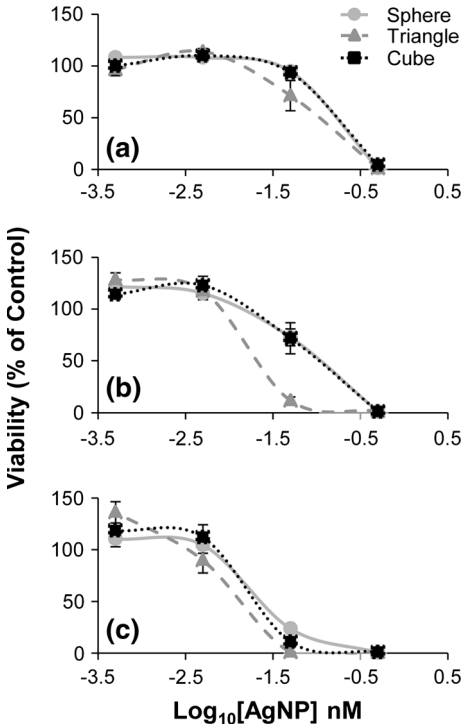

Fig. 4 Viability, normalized to the control, of hFOB cells after exposure to sAgNP, tAgNP, and cAgNP after **a** 24 h, **b** 3 days, and **c** 5 days

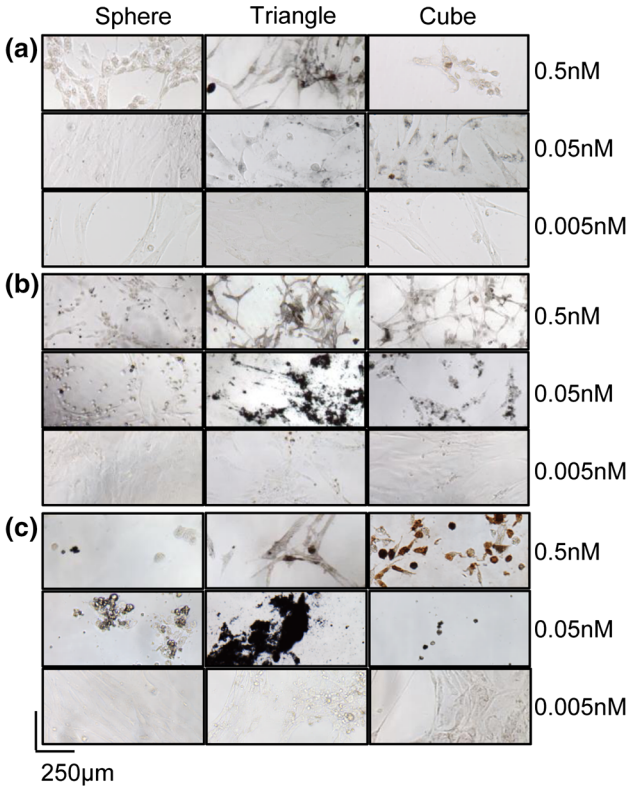

Fig. 5 Light micrographs of hFOB cells exposed to sAgNP, tAgNP, and cAgNP at a range of concentrations (0.5, 0.05, and 0.005 nM) after **a** 24 h, **b** 3 days, and **c** 5 days

indicated that the lower AgNPs concentrations have minimal effects on *S. aureus* bacteria. Contradicting this observation, a study by Panáček and co-workers reported that the minimum inhibitory concentration was found to be at a low concentration of 6.75 μg/ml [24]. Furthermore, it was observed from our study that geometry of AgNPs had no effect on the susceptibility of *S. aureus* or MRSA. There was, however, an observed trend of slightly greater susceptibility of MRSA to cAgNPs. Using *E. coli*, Pal et al. reported that the tAgNPs was more susceptible when compared to the sAgNPs [15]. Differences in observations could also be attributed to the synthesis process; in this study the PVP acted as both a reducing and capping agent resulting in a PVP coated particle whereas the AgNPs synthesized by Pal et al. did not contain a capping agent. However, the observations from this study and that of Pal et al. both suggest that the susceptibility of bacteria to AgNPs is species dependent.

Although it was also observed from this study that hFOB viability was not affected by AgNP geometry, these nanoparticles did confer a time-dependent response on the hFOB. This observation was in agreement with a study by Pauksch et al. in which both a dose- and time-dependent reduction in cell viability was observed when the osteoblasts and mesenchymal stem cells were exposed to AgNPs at different concentration over a 21 day period [25]. In our study it was observed that the cells exhibited 0 % viability as compared to the control after a 24 h exposure to the AgNPs at a concentration of 0.5 nM. When exposed to tAgNPs at a concentration of 0.05 nM, cell viability was lower as compared to that of cells exposed to sAgNPs or cAgNPs at the same concentration. At lower concentrations, the viability of the cells was unchanged as compared to the control. However, after 3 days of exposure, a decrease in cell viability was observed for cells exposed to the AgNPs at a concentration of 0.05 nM, with a significant change in viability for cells exposed to the tAgNPs. There was also an observed increase in cell viability after 3 days of exposure to AgNPs at concentrations of 0.005 nM and below. This observed effect of enhance proliferation over the control at low AgNP doses was also reported by Kawata et al., with HepG2 human hepatoma cells experiencing accelerated proliferation after exposure to AgNPs at low doses (<0.5 mg/l) [6]. This enhancement of proliferation was suggested to be a result of the upregulation of DNA repair-associated genes in response to DNA damaging effects. By day 5, the hFOB exposed to low AgNPs concentrations (<0.005 nM) showed no loss in cell viability.

It was also observed from this study that the decrease in cell viability to AgNPs was associated with a change in cell

morphology. Cells exposed to the low AgNP concentrations over a 5 day period were observed to maintain normal cell spreading and elongated cell morphology. However, at the highest concentration used in this study, changes in cell morphology were observed. The cAgNPs were observed to affect the cells after 24 h exposure, causing the cells to shrink and have irregular morphologies. In comparison to cAgNPs, the tAgNPs and sAgNPs were not observed to have such dramatic effect after 24 h exposure, with the cells exhibiting an elongated morphology. However, by day 3, the cells exposed to tAgNPs and sAgNPs exhibited shrinkage with irregular morphologies. By day 5, there was an apparent accumulation of AgNPs in cells exposed to cAgNPs or tAgNPs, thereby possibly explaining their change in morphology and low viability. Furthermore, it has also been suggested that nanoparticles can be internalized by mesenchymal stem cells such as bone marrow cells, and depends on many factors such as cell type and the shape and chemistry of the nanoparticles [26]. Thus, the mechanism of action cellular uptake of these nanoparticles and their effect on cellular behavior will be evaluated in future studies.

5 Conclusion

Direct exposure of AgNPs can substantially affect the viability of the microbial cultures. However, it was also concluded from these studies that the geometry of the AgNPs did not significantly impact the susceptibility outcome of the attached *S. aureus* and MRSA for subsequent biofilm formation. Furthermore, while lower AgNP concentrations did not affect the hFOB viability, it was also concluded that the presence of AgNPs results in a time-dependent reduction in hFOB population over time.

Compliance with Ethical Standards

Conflict of interest The authors declare no conflict of interest.

References

1. Campoccia D, Montanaro L, Arciola CR. A review of the clinical implications of anti-infective biomaterials and infection-resistant surfaces. Biomaterials. 2013;34:8018–29.
2. Evan M, Hetrick MHS. Reducing implant-related infections: active release strategies. Chem Soc Rev. 2006;35:780–9.
3. Romeo T, editor. Bacterial biofilms. Current topics in microbiology and immunology, vol. 322. Berlin: Springer; 2008.
4. Trampuz A, Widmer AF. Infections associated with orthopedic implants. Curr Opin Infect Dis. 2006;19:349–56.
5. Flemming H-C. Biofilm highlights. Springer Series on Biofilms. New York: Springer; 2011.
6. Kawata K, Osawa M, Okabe S. In vitro toxicity of silver nanoparticles at noncytotoxic doses to HepG2 human hepatoma cells. Environ Sci Technol. 2009;43(15):6046–51.
7. Zimmerli W. Prosthetic-join-associated infections. Best Pract Res Clin Rheumatol. 2006;20(6):1045–63.
8. Ribeiro M, Monteiro FJ, Ferraz MP. Infection of orthopedic implants with emphasis on bacterial adhesion process and techniques used in studying bacterial-material interactions. Biomatter. 2012;2(4):176–94.
9. Leid JG, Leid J, Shirtliff M, editors. The role of biofilm in device-related infections. Springer Series on Biofilms. Los Angeles: Springer; 2009.
10. Vasilev K, Cook J, Griesser HJ. Antibacterial surfaces for biomedical devices. Exp Rev Med Devices. 2009;6(5):553–67.
11. Lara HH, Garza-Treviño EN, Ixtepan-Turrent L, Singh DK. Silver nanoparticles are broad-spectrum bactericidal and virucidal compounds. J Nanobiotechnol. 2011;9(1):30.
12. Tran QH, Le AT. Silver nanoparticles: synthesis, properties, toxicology, applications and perspectives. Adv Nat Sci Nanosci Nanotechnol. 2013;4:033001.
13. Dal Lago V, de Oliveira LF, de Almeida Gonçalves K, Kobarg J, Cardoso MB. Size-selective silver nanoparticles: future of biomedical devices with enhanced bactericidal properties. J Mater Chem. 2011;21(33):12267–73.
14. Marambio-Jones C, Hoek EM. A review of the antibacterial effects of silver nanomaterials and potential implications for human health and the environment. J Nanopart Res. 2010;12:1531–51.
15. Pal S, Tak YK, Song JM. Does the antibacterial activity of silver nanoparticles depend on the shape of the nanoparticle? A study of the gram-negative bacterium *Escherichia coli*. Appl Environ Microbiol. 2007;73(6):1712–20.
16. Metraux GS, Mirkin CA. Rapid thermal synthesis of silver nanoprisms with chemically tailorable thickness. Adv Mater. 2005;17(4):412–5.
17. Sun Y, Xia Y. Shape-controlled synthesis of gold and silver nanoparticles. Science. 2002;298:2176–9.
18. Yguerabide J, Yguerabide EE. Light-scattering submicroscopic particles as highly fluorescent analogs and their use as tracer labels in clinical and biological applications. Anal Biochem. 1998;262:137–56.
19. Chen Z, Gao L. A facile and novel way for the synthesis of nearly monodisperse silver nanoparticles. Mater Res Bull. 2007;42:1657–61.
20. Mansouri SS, Ghader S. Experimental study of effect of different parameters on size and shape of triangular silver nanoparticles prepared by a simple and rapid method in aqueous solution. Arab J Chem. 2009;2:47–53.
21. Chen S, Carroll DL. Silver nanoplates: size control in two dimensions and formulation mechanism. J Phys Chem B. 2004;108:5500–6.
22. Skrabalak SE, Au L, Li X, Xia Y. Facile synthesis of Ag nanocubes and Au nanocages. Nat Protoc. 2007;2(9):2182–90.
23. Mdluli PS, Sosibo NM, Mashazi PN, Nyokong T, Tshikhudo RT, Skepu A, Van Der Lingen E. Selective adsorption of PVP on the surface of silver nanoparticles: a molecular dynamics study. J Mol Struct. 2011;1004:131–7.
24. Kvitek L, Panáček A, Soukupova J, Kolar M, Vecerova R, Prucek R, et al. Effect of surfactants and polymers on stability and antibacterial activity of silver nanoparticles (NPs). J Phys Chem C. 2008;112:5825–34.
25. Pauksch L, Hartmann S, Rohnke M, Szalay G, Alt V, Schnettler R, Lips KS. Biocompatibility of silver nanoparticles and silver ions in primary human mesenchymal stem cells and osteoblasts. Acta Biomater. 2014;10:439–49.
26. Tautzenberger A, Kovtun A, Ignatius A. Nanoparticles and their potential application in bone. Int J Nanomed. 2012;7:4545–57.